

Half-metallicity and giant magneto-optical Kerr effect in N-doped NaTaO₃

Y. Saeed¹, N. Singh^{1,2}, and U. Schwingenschlgl¹

¹*Physical Science & Engineering division, KAUST,
Thuwal 23955-6900, Kingdom of Saudi Arabia and*

²*Solar and Photovoltaic Energy Research Center,
KAUST, Thuwal 23955-6900, Kingdom of Saudi Arabia*

Abstract

We employ density functional theory using the modified Becke-Johnson (mBJ) approach to investigate the electronic and magneto-optical properties of N-doped NaTaO₃. The mBJ results reveal a half metallic nature of NaTaO₂N, in contrast to results obtained by the generalized gradient approximation. We find a giant polar Kerr rotation of 2.16° at 725 nm wave length (visible region), which is high as compared to other half metallic perovskites as well as to the prototypical half metal PtMnSb.

I. INTRODUCTION

Room temperature ferromagnetism has been reported for different doped oxides such as C/N-doped ZnO [1–3], TiO₂ [4–6], SnO₂ [7, 8] and confirmed recently [9–11]. Room temperature ferromagnetism with half metallicity is reported for N-doped SrTiO₃ and BaTiO₃ [12, 13], in which the magnetic interactions between the nearest and next-nearest N dopants result in a strong ferromagnetic coupling [14]. Ferromagnetic half-metals have potential applications in spintronics devices [15, 16] and also show unusual magneto-optical effects due to a metallic state for one spin channel and an insulating state for the other. Yang *et al.* have reported that a high concentration of N is required for achieving a magnetic long range order in perovskite oxide [14].

The perovskite oxide NaTaO₃ (NTO) is a ferroelectric material with high permittivity and low dielectric loss, which suggests usage in microwave devices [17–19]. Several ab-initio calculations have been performed to describe the electronic properties of bulk NTO [20] but a detailed study of the electronic structure and magneto-optical properties of N-doped NTO is missing in the literature. The magneto-optical Kerr effect of doped NTO is interesting for magneto-optical reading and recording devices [21]. The N-doped perovskite oxide NTO is a 5d system. Therefore, electron correlation effects are expected to be small as compared to 3d systems such as SrTiO₃ and BaTiO₃. In the following we establish a half metallic nature for NaTaO_{1-x}N_x ($x = 0.04 - 0.33$) and discuss the electronic structure in comparison to the strongly correlated perovskites SrTiO₃ and BaTiO₃. We also address the magneto-optical Kerr effect in N-doped NTO.

II. COMPUTATIONAL METHOD

Our calculations are based on density functional theory, using the full-potential linearized augmented plane wave approach as implemented in the WIEN2k code [22]. We use the modified Becke-Johnson (mBJ) exchange correlation potential [23]. The popular generalized gradient approximation (GGA) [24] is employed to optimize the volume and the internal atomic coordinates. In general, the unit cell is divided into non-overlapping atomic spheres centered at the atomic sites and an interstitial region. The convergence parameter $R_{mt}K_{max}$, where K_{max} is the plane-wave cut-off and R_{mt} is the smallest muffin-tin radius, controls the

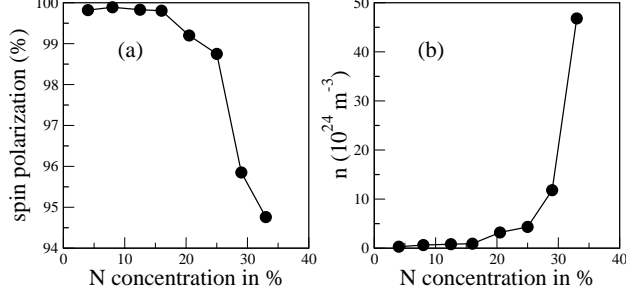


FIG. 1: Calculated spin polarization and majority spin hole density n as a function of N-concentration, as obtained by the GGA+SOC approximation.

size of the basis set. This convergence parameter is set to 7 together with $G_{max} = 24$. We use 66 \mathbf{k} -points in the irreducible wedge of the Brillouin zone for calculating the electronic structure and a dense mesh of 480 \mathbf{k} -points in the magneto-optical calculations. The cubic phase $Pm\bar{3}m$ ($a = b = c = 3.93 \text{ \AA}$ and $\alpha = \beta = \gamma = 90^\circ$) of NTO [25] is used in the present calculations for simplicity because the differences to the monoclinic phase $P2_1/m$ ($a = 3.8995 \text{ \AA}$, $b = 3.8965 \text{ \AA}$, and $c = 3.8995 \text{ \AA}$, $\alpha = \gamma = 90^\circ$, and $\beta = 90.15^\circ$) are subordinate [26]. As a consequence, the electronic band structures and density of states (DOS) are found to be very similar in both phases [27, 28].

III. RESULTS AND DISCUSSION

Our optimized lattice parameter (using the GGA) of cubic NTO is 3.98 \AA , which is in good agreement with the experimental value of 3.93 \AA [25]. We replace one O with one N to form the oxynitrate (NaTaO_2N). The optimized lattice parameters of NaTaO_2N is slightly increased to 4.03 \AA . In order to find the magnetic ground state, we construct a $1 \times 1 \times 2$ supercell using the optimized structure and replace two O atoms with N. We compare the ground state energies of ferromagnetic (FM) and anti-ferromagnetic (AFM) configurations. The magnetic energy $E_{mag} = E_{FM} - E_{AFM} = -51.3 \text{ meV}$, and the N-N distance is $\sim 4 \text{ \AA}$ with a total magnetic moment of $2 \mu_B$ per cell (or $1 \mu_B$ per N atom) in FM case. The Curie temperature T_C is calculated using the mean-field Heisenberg model, i.e., $T_C = (2/3)E_{mag}/k_B$ [29, 30]. The calculated T_C for NaTaO_2N is 396 K, which is close to that of N-doped SrTiO_3 and BaTiO_3 at the same N-N distance [14]. In order to observe the long range FM order, we study a high N-doping of 33% by replacing one O by one N

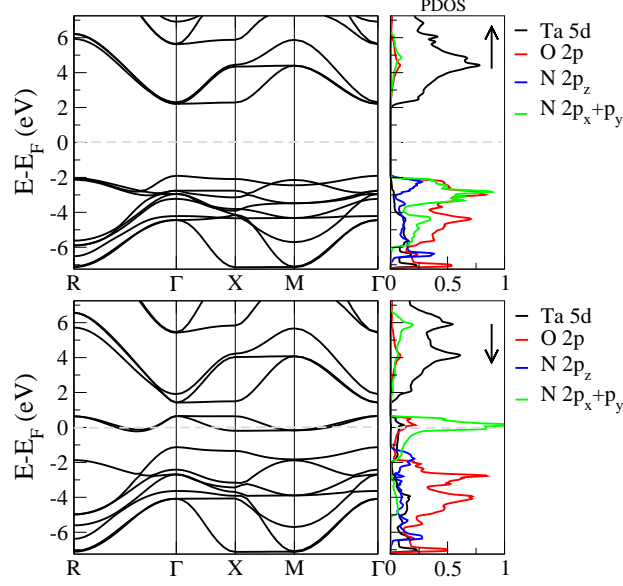


FIG. 2: Band structure and DOS of NaTaO₂N as obtained by the mBJ approximation.

in a single unit cell. A magnetic moment is induced as the delocalized N p states become polarized, where $0.15 \mu_B$ come from the interstitial, $0.13 \mu_B$ come from O and $0.61 \mu_B$ come from N, summing upto $1 \mu_B$ per N atom.

To explain the induced spin-polarization in NaTaO₂N, we analyze DOS and electronic band structure obtained by GGA approximation (not shown here). The DOS shows a half-metallic character with a metallic state for the minority spin and an insulating state for the majority spin. To confirm the half-metallicity, we include spin orbit coupling (SOC) along with GGA in the calculations, finding that NaTaO₂N becomes a metal since the majority spin states cross the Fermi level. The spin polarization ($= \frac{N_{\uparrow} - N_{\downarrow}}{N_{\uparrow} + N_{\downarrow}}$, where N is the number of states at the Fermi level) of NaTaO₂N is obtained $\sim 94\%$. In order to find the exact N-concentration at which the character of the system changes from a half-metal to metal, we construct a $3 \times 3 \times 3$ supercell and vary the N-concentration from 4% to 33% (including SOC in the calculations). In Fig. 1(a), we plot the spin-polarization as a function of the N-concentration. Below 16% N-doped, NTO shows a $\sim 99.8\%$ spin-polarization which decreases sharply to $\sim 94\%$ at 33% N-doping. In Fig. 1(b), we plot the hole density (holes per volume) for the majority spin channel. Similar to the spin-polarization, the hole density increases rapidly upto $46.8 \times 10^{24} \text{ m}^{-3}$ as the N-concentration increases to 33%, while the hole density is almost constant for low N-concentration.

Recently, Guo *et al.* [31] have applied the mBJ approach successfully to improve the

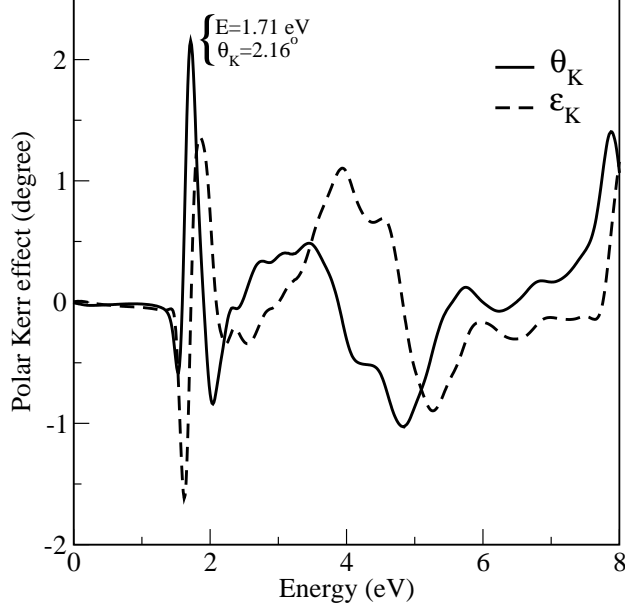


FIG. 3: Calculated polar Kerr angle θ_K and Kerr ellipticity ϵ_K of NaTaO₂N.

half-metallic ferromagnetism in zincblende MnAs, which turns into a half-metal without affecting the $d\ t_{2g}$ bands. We apply the same method to NaTaO₂N. The calculated band structure and DOS in Fig. 2 show a truly half-metallic nature for NaTaO₂N. The majority spin bands are similar to pristine NTO with a gap of 3.96 eV, which is in excellent agreement with experiments [28] and the previous GW calculations [27]. The minority spin channel is metallic due to a non-zero DOS at the Fermi level. The band splitting at the Fermi level along R- Γ and M- Γ is very small, while along Γ -X-M, it is large. The calculated plasma frequency ω_p from the minority spin channel due to metallic nature, is 2.7 eV, which is smaller in the ferromagnetic half-metal PtMnSb ($\omega_p = 4.5$ eV) [32], reflecting less dispersed bands. The calculated DOS shows that the valence bands (majority spin) are a combination of N 2*p* and O 2*p* states. The bottom of the conduction bands is composed of Ta 5*d* states (see Fig. 2). For the minority spin channel, the N 2*p* bands cross the Fermi level (with small O 2*p* contributions). The N 2*p*^{↑↓} states split into $(p_x + p_y)^{\uparrow\downarrow}$ and $p_z^{\uparrow\downarrow}$ bands. There is no shifting of peak position with respect to energy is observed at the Fermi level in N 2 $(p_x + p_y)^{\uparrow\downarrow}$ and N 2*p*_{*z*}^{↑↓} states from the N-doped SrTiO₃ and BaTiO₃ [14] where N 2*p*_{*y*} + *p*_{*z*} and N 2*p*_{*x*} have different peak position at the Fermi level. There is a strong hybridization between the N 2*p*^{↑↓} and O 2*p*^{↑↓} states for the minority spin channel. The Ta 5*d*^{↑↓} bands do not change with the N-concentration.

Intense search aim at materials with large magneto-optical peaks in the low wave-length region to be used for high-density storage [33]. Both borates [34] and Zintl compounds [35, 36], can shows a remarkable Kerr signal in the low energy range. The Kerr rotation θ_K and Kerr ellipticity ε_K of half metallic NaTaO₂N are shown in Fig. 3. We find a value of $\theta_K = 2.16^\circ$ at 1.71 eV (~ 725 nm), which is higher than in BiNiO₃ ($\theta_K = 1.28^\circ$) [37] and the Heusler compound PtMnSb ($\theta_K = 1.27^\circ$) [38, 39]. The high Kerr angle is an intraband effect, and not due to the SOC (which creates an imbalance in the optical transitions in PtMnSb and NiMnSb [40], for example. For the minority spin channel, the band structure of NaTaO₂N shows a set of parallel bands across the Fermi level (R- Γ , Γ -X-M, and Γ -M) which consist of N $2(p_x + p_y)^\downarrow$ states. These parallel bands give rise to intraband transitions which contribute significantly to the Kerr spectrum in the low energy range. In NaTaO₂N, the separation between these bands is much smaller than in PtMnSb [40]. This past explain the higher magneto-optical Kerr effect in NaTaO₂N. The calculated Kerr ellipticity ε_K has a maximum of $\sim 1.7^\circ$ at 1.6 eV.

IV. CONCLUSION

In conclusion, we have presented first principles results of the band structure, DOS, and magneto-optical properties of N-doped NaTaO₃, as obtained from density functional theory. Our results for NaTaO_{1-x}N_x ($x = 0.04 - 0.33$) show that the GGA+SOC approach gives a 99% spin-polarization at low N-concentrations upto 16%. The mBJ+SOC approach results in a pure ferromagnetic half-metal in contrast to the GGA+SOC. We observe a giant magneto-optical Kerr signal of $\theta_K=2.16^\circ$ at ~ 725 nm in NaTaO₂N, which is the highest Kerr angle among the ferromagnetic half-metals in UV-visible region. The origin of the high Kerr angle is attributed to intraband transitions involving the N $2(p_x + p_y)^\downarrow$ orbital due to parallel bands around the Fermi level. The large Kerr rotation in NaTaO₂N in the visible region may find applications in red/infrared laser magneto-optical devices and the half metallic nature of NaTaO₂N is interesting for spintronics devices.

-
- [1] H. Pan, J. B. Yi, L. Shen, R. Q. Wu, J. H. Yang, J. Lin, Y. P. Feng, J. Ding, L.H. Van, and J. H. Yin, Phys. Rev. Lett. 99, 127201 (2007).

- [2] L. Shen, R. Q. Wu, H. Pan, G. W. Peng, M. Yang, Z. D. Sha, and Y. P. Feng, Phys. Rev. B 78, 073306 (2008).
- [3] K. Yang, R. Wu, L. Shen, Y. P. Feng, Y. Dai, and B. Huang, Phys. Rev. B 81, 125211 (2010).
- [4] K. Yang, Y. Dai, B. Huang, and M.-H. Whangbo, Appl. Phys. Lett. 93, 132507 (2008).
- [5] K. Yang, Y. Dai, B. Huang, and M.-H. Whangbo, Chem. Phys. Lett 481, 99 (2009).
- [6] J. G. Tao, L. X. Guan, J. S. Pan, C. H. A. Huan, L. Wang, J. L. Kuo, Z. Zhang, J. W. Chai, and S. J. Wang, Appl. Phys. Lett. 95, 062505 (2009).
- [7] G. Rahman and V. M. García-Suárez, Appl. Phys. Lett. 96, 052508 (2010).
- [8] W.-Z. Xiao, L.-L. Wang, L. Xua, Q. Wan, and B. S. Zou, Solid State Commun. 149, 1304 (2009).
- [9] B. J. Nagare, S. Chack, and D. G. Kanhere, J. Phys. Chem. A 114, 2689 (2010).
- [10] N. N. Bao, H. M. Fan, J. Ding, and J. B. Yi, J. Appl. Phys. 109, 07C302 (2011).
- [11] N. H. Hong, J.-H. Song, A. T. Raghavender, T. Asaeda, and M. Kurisu, Appl. Phys. Lett. 99, 052505 (2011).
- [12] C. M. Liu, X. Xiang, and X. T. Zu, Chin. J. Phys. 47, 893 (2009).
- [13] X. Tan, C. Chen, K. Jin, and B. Luo, J. Alloy. Compd. 509, L311 (2011).
- [14] K. Yang, Y. Dai, and B. Huang, Appl. Phys. Lett. 100, 062409 (2012).
- [15] P. G. van Engen, K. H. J. Buschow, and R. Jongebreur, Appl. Phys. Lett. 42, 202 (1982).
- [16] R. A. de Groot, F. M. Mueller, P. G. van Engen, and K. H. J. Buschow, Phys. Rev. Lett. 50, 2024 (1983).
- [17] K. Rabe, C. H. Ahn, and J.-M. Triscone, Physics of Ferroelectrics: A Modern Perspective, Topics in Applied Physics (Springer, Berlin, 2007), Vol. 105.
- [18] R. G. Geyer, B. Riddle, J. Krupka, and L. A. Boatner, J. Appl. Phys. 97, 104111 (2005).
- [19] A.-K. Axelsson, Y. Pan, M. Valant, and N. Alford, J. Am. Ceram. Soc. 92, 1773 (2009).
- [20] M. Choi, F. Oba, and I. Tanaka, Phys. Rev. B 83, 214107 (2011).
- [21] M. Fiebig, J. Phys. D: Appl. Phys. 38, R123 (2005).
- [22] P. Blaha, K. Schwarz, G. Madsen, D. Kvasicka, and J. Luitz, WIEN2k, An Augmented Plane Wave + Local Orbitals Program for Calculating Crystal Properties (TU Vienna, Vienna, 2001).
- [23] F. Tran and P. Blaha, Phys. Rev. Lett. 102, 226401 (2009).
- [24] J. P. Perdew, K. Burke, and M. Ernzerhof, Phys. Rev. Lett. 77, 3865 (1996).

- [25] International Center for Diffraction Data, JCPDS Card No. 742488 (2001).
- [26] International Center for Diffraction Data, JCPDS Card No. 742479 (2001).
- [27] H. Wang, F. Wu, and H. Jiang, *J. Phys. Chem. C* 115, 16180 (2011).
- [28] W. H. Lin, C. Cheng, C. C. Hu, and H. Teng, *Appl. Phys. Lett.* 89, 211904 (2006).
- [29] J. Kudrnovský, I. Turek, V. Drchal, F. Máca, P. Weinberger, and P. Bruno, *Phys. Rev. B* 69, 115208 (2004).
- [30] F. Máca, J. Kudrnovský, V. Drchal, and G. Bouzerar, *Appl. Phys. Lett.* 92, 212503 (2008).
- [31] S.-D. Guo and B.-G. Liu, *Euro. Phys. Lett.* 93, 47006 (2011).
- [32] S. Picozzi, A. Continenza, and A. J. Freeman, *J. Phys. D: Appl. Phys.* 39, 851 (2006).
- [33] P. J. Grundy, in *Electronic and Magnetic Properties of Metals and Ceramics, Materials Science and Technology*, edited by K. H. J. Buschow (VCH, 1994), Vol. 3B, p. 575.
- [34] Y. Saeed, N. Singh, and U. Schwingenschlögl, *J. Appl. Phys.* 110, 103512 (2011).
- [35] N. Singh and U. Schwingenschlögl, *Chem. Phys. Lett.* 508, 29 (2011).
- [36] N. Singh and U. Schwingenschlögl, *Appl. Phys. Lett.* 100, 151906 (2012).
- [37] M. Q. Cai, X. Tan, G. W. Yang, L. Q. Wen, L. L. Wang, W. Y. Hu, and Y. G. Wang, *J. Phys. Chem. C* 112, 16638 (2008).
- [38] P. G. van Engen, K. H. J. Buschow, R. Jongebreur, and M. Erman, *Appl. Phys. Lett.* 42, 202 (1983).
- [39] I. D. Lobov, A. A. Makhnev, and M. M. Kirillova, *Phys. Met. Metallogr.* 113, 135 (2012), and references therein.
- [40] J. van Ek and J. M. Maclaren, *Phys. Rev. B* 56, R2924 (1997).